

GarNet: A Two-stream Network for Fast and Accurate 3D Cloth Draping

Erhan Gundogdu¹, Victor Constantin¹, Amrollah Seifoddini²
 Minh Dang², Mathieu Salzmann¹, Pascal Fua¹

¹CVLab, EPFL, Switzerland

²Fision Technologies, Zurich, Switzerland

{erhan.gundogdu, victor.constantin, mathieu.salzmann, pascal.fua}@epfl.ch
 {amrollah.seifoddini, minh.dang}@fision-technologies.com

Abstract

While *Physics-Based Simulation (PBS)* can highly accurately drape a 3D garment model on a 3D body, it remains too costly for real-time applications, such as virtual try-on. By contrast, inference in a deep network, that is, a single forward pass, is typically quite fast. In this paper, we leverage this property and introduce a novel architecture to fit a 3D garment template to a 3D body model. Specifically, we build upon the recent progress in 3D point-cloud processing with deep networks to extract garment features at varying levels of detail, including point-wise, patch-wise and global features. We then fuse these features with those extracted in parallel from the 3D body, so as to model the cloth-body interactions. The resulting two-stream architecture is trained with a loss function inspired by physics-based modeling, and delivers realistic garment shapes whose 3D points are, on average, less than 1.5cm away from those of a PBS method, while running 40 times faster.



Figure 1: **Simulating a T-Shirt and Jeans. Left:** Our network. **Right:** Physics-Based Simulation.

1. Introduction

Garment simulation is useful for many purposes such as virtual try-on, online shopping, gaming, and virtual reality. Physics-Based Simulation (PBS) can deliver very high realism but at a heavy computational cost that makes it unsuitable for real-time and web-based applications. In this paper, we propose to train a deep network to learn to reproduce the output of a PBS method in real time on an ordinary GPU-equipped machine while still modeling fine details such as the wrinkles and folds as shown in Fig. 1.

Realistic simulation of cloth draping over the human body requires accounting for the global 3D pose of the person and for the local interactions between skin and cloth caused by the body shape. To this end, we introduce the architecture depicted by Fig. 2. It consists of a Garment stream and a Body stream. The Body one uses a Point-

Net [24] inspired architecture to extract local and global information about the person. The Garment stream exploits the global body features to compute point-wise, patch-wise and global features for the garment mesh. These features, along with the global body ones, are then fed to a fusion subnetwork to predict the shape of the fitted garment. In one implementation of our approach, shown in Fig. 2(a), the local body features are only used *implicitly* to compute the global ones. In a second implementation, we *explicitly* take them into account to further model the skin-cloth interactions. To this end, we introduce an auxiliary stream that first computes the K nearest body vertices to each garment vertex, performs feature pooling on point-wise body features and finally feeds them to the fusion subnetwork. This more sophisticated version is depicted by Fig. 2(b). We will

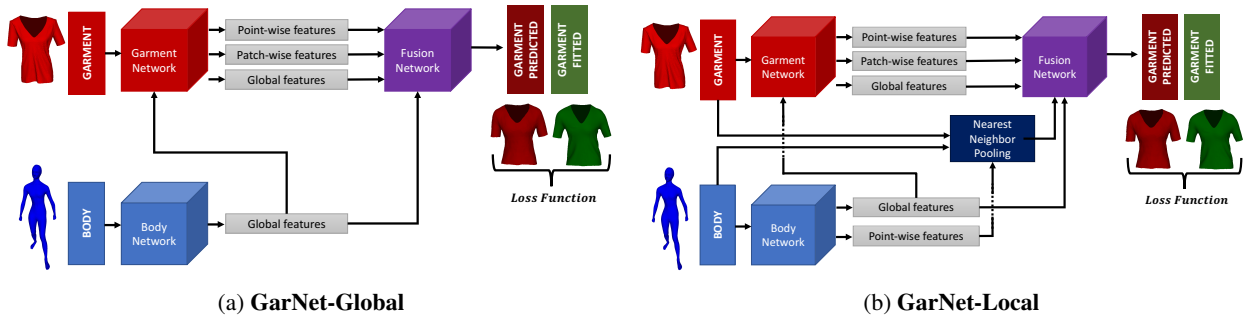


Figure 2: **Two versions of our two-stream garment fitting architecture.** (**GarNet-Global**): We fuse the global body features with the garment features both early and late. (**GarNet-Local**) In addition, we use a nearest neighbor approach to pooling local body features and feed the result to the fusion network whose job is to combine the body and garment features.

see that it performs only slightly better than the simpler one, indicating that the so-called global body features already capture enough local information for our purposes.

By incorporating appropriate loss terms in the objective function we minimize during training, at test time, we avoid the need for extra post-processing steps to prevent cloth-body interpenetration and undue tightness that PBS tools [20, 26, 21, 7], optimization-based [4] and data-driven [9] methods often require. Furthermore, these data-driven methods are typically limited by their use of low-dimensional parametric representations to remain scalable. By contrast, our network can handle meshes of arbitrary size by performing point-wise prediction.

Our contribution is therefore a novel architecture for garment simulation that delivers realism in real time by properly modeling the body and garment interaction, thus preventing cloth and body interpenetration. For training purposes, we built a dataset which comprises 6000 female jeans, 7350 male jeans, 8000 female t-shirts, and 9800 male t-shirts worn by animated bodies from the CAESAR dataset [1]. Whereas the PBS approach takes about 2 seconds per frame to predict the shape of a garment, ours takes less than 50 milliseconds. Furthermore, we show that our approach outperforms the very recent one of [28], that also employs a deep network model, on their own dataset.

2. Related Work

Many professional tools can model cloth deformations realistically using Physics-Based Simulation (PBS) [20, 26, 21, 7]. However, they are computationally expensive, which precludes real-time use. Furthermore, manual parameter tuning is often required. In this section, we briefly review recent approaches to overcoming these limitations.

Data-Driven Approaches. They are less computationally intensive and memory demanding, at least at run-time, and have emerged as viable competitors to PBS. In one of the early methods [14], a set of garment-body pairs is gener-

ated, and at test time they predict the garment shapes in an unseen pose by linearly interpolating the garments in the database. In [10], potential wrinkles for each body joint are stored in a database so as to model fine details in various body poses. However, it requires performing this operation for each body-garment pair. To speed up the computation, [8] models the relation between 2D cloth deformations and corresponding bodies in a low-dimensional space. [9] extends this idea for 3D shapes by factorizing the cloth deformations according to what causes them—changes in body shape and pose mostly—and the factorized model is trained to predict the garment’s final shape. However, an *a posteriori* refinement is still needed to impose smoothness and to prevent cloth-body interpenetration. The much more recent approach of [28] relies on a deep encoder-decoder model to create a joint representation for bodies, garment sewing patterns, 2D sketches and garment shapes. This defines a mapping between any pair of such entities, for example body-garment shape. However, it relies on a Principal Component Analysis (PCA) representation of the garment shape, thus yielding limited shape accuracy. In contrast to [28], our method operates directly on the body and garment meshes, removing the need for a potentially limiting latent representation.

Cloth fitting can also be performed by using 4D scan data as in [16, 23]. In [23], garments deforming over time are reconstructed using 4D scanning data and the reconstructions are then retargeted to other bodies without accounting for physics-based clothing dynamics. Unlike [23], we aim not only to obtain visually plausible results but also to emulate PBS for cloth fitting. In [16], fine wrinkles are generated by a conditional Generative Adversarial Network (GAN) that takes as input predicted, low-resolution normal maps. This method, however, requires an additional step to register the template cloth to the captured 4D scan, while ours requires no extra processing steps.

Point Cloud and Mesh Processing. A key innovation that has made our approach practical is the recent emergence of deep architectures that allow for the processing of unstructured point clouds [24, 25] and meshes [27]. PointNet [24, 25] was the first to efficiently represent and use unordered point clouds for 3D object classification and segmentation. It has spawned several approaches to point-cloud upsampling [31], unsupervised representation learning [29], 3D descriptor matching [6], and finding 2D correspondences [30]. In our architecture, as in PointNet, we use Multilayer Perceptrons (MLPs) for point-wise processing and global feature generation.

When the topology of the point clouds is specified, for example in the form of a triangulated mesh, graph convolution methods can be used [3, 17, 18] using hand-crafted patch operators. FeatNet [27] generalizes this approach by learning how to dynamically associate convolutional filter weights with features at the vertices of the mesh, and demonstrates state-of-the-art performance on the 3D shape correspondence problem. We also use mesh convolutions to extract patch-wise garment features that encode the neighborhood geometry. A key difference from these techniques, however, is that we do not work with a single point cloud or mesh as input, but with two: one for the body and the other for the garment, which are combined in our proposed two-stream architecture.

3. 3D Garment Fitting

To fit a garment to a body in a specific pose, we start by using a dual quaternion skinning (DQS) method [13] that produces a rough initial garment shape depending only on the body pose. We then introduce two variants of our **GarNet** deep network to refine this initial shape and produce the final garment result. Fig. 2 depicts these two variants. We now formalize the problem and describe our network’s components in the remainder of the section.

3.1. Formalization

Let \mathcal{M}^0 be the template garment mesh in the rest pose and let $\mathcal{M} = \text{dqs}(\mathcal{M}^0, \mathcal{B})$ be the garment after skinning to the body \mathcal{B} , also modeled as a mesh. Let f_θ denote the network with weights θ chosen so that the predicted garment \mathcal{G}^P given \mathcal{M} and \mathcal{B} is as close as possible to the ground-truth shape \mathcal{G}^G . We denote the i^{th} vertex of \mathcal{M} , \mathcal{B} , \mathcal{G}^G and \mathcal{G}^P by \mathbf{M}_i , \mathbf{B}_i , \mathbf{G}_i^G and $\mathbf{G}_i^P \in \mathbb{R}^3$, respectively. Finally, let N be the number of vertices in \mathcal{M} , \mathcal{G}^G and \mathcal{G}^P .

Since predicting deformations from a reasonable initial shape is much simpler than predicting absolute 3D locations, we train f_θ to predict a translation vector for each vertex of the warped garment \mathcal{M} that brings it as close as possible to the corresponding ground-truth vertex. In other

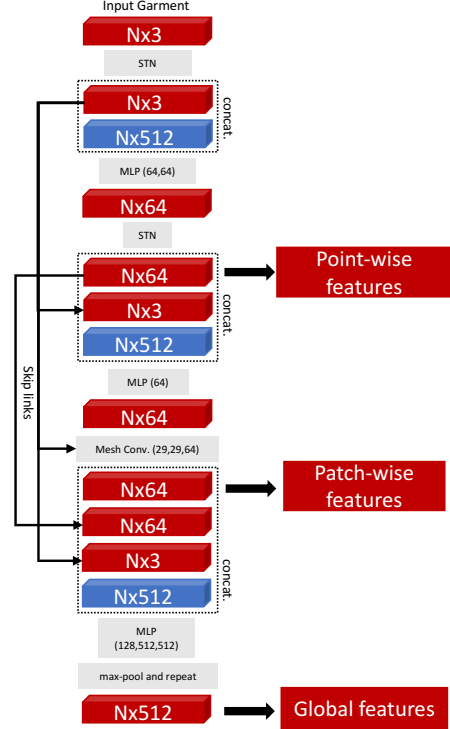


Figure 3: **Garment branch of our network.** The grey boxes denote network layers while red and blue ones represent garment and global body features, respectively. STN stands for a Spatial Transformer Network used in PointNet [24]. We use rectified linear units (ReLU) after each MLP block and mesh convolution layer.

words, we optimize with respect to θ so that

$$\mathcal{T}^P = f_\theta(\mathcal{M}, \mathcal{B}) \approx \mathcal{T}^G, \quad (1)$$

where \mathcal{T}^P and \mathcal{T}^G correspond to translation vectors from the predicted and ground-truth mesh to the corresponding skinned garment \mathcal{M} , that is, $\mathbf{G}_i^P - \mathbf{M}_i$ and $\mathbf{G}_i^G - \mathbf{M}_i$, respectively. Therefore, the final shape of the garment mesh is obtained by adding the translation vectors predicted by the network to the vertex positions after skinning.

3.2. Network Architecture

Fig. 2 describes two variants of the two-stream architecture we use to compute $f_\theta(\mathcal{M}, \mathcal{B})$. We now describe them in more detail. Their architecture consists of a Body and a Garment stream, whose outputs are fed into a fusion network that relies on a set of MLP blocks to produce the predicted set of translations \mathcal{T}^P of Eq. 1. To not only produce a rough garment shape, but also predict fine details such as wrinkles and folds, we include early connections between the two streams, allowing the Garment stream to account for the body shape even when processing local information. This process is discussed in more detail below.

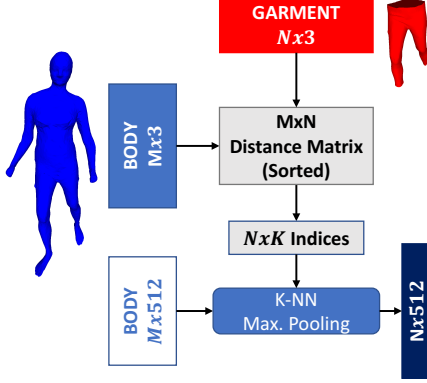


Figure 4: **K nearest neighbor pooling.** We compute the K nearest neighbor body vertices of each garment vertex and max-pool their local features.

Body Stream. The first stream processes the body \mathcal{B} in a similar way to PointNet [24] to efficiently produce point-wise and global features that adequately represent body pose and shape. Since the vertices of body and garment meshes do not have a direct correspondence, the global body features are key to incorporating such information when processing the garment.

Garment Stream. The second stream takes as input the warped garment \mathcal{M} and the global body features extracted by the Body stream to also compute point-wise and global features. As we will see in the results section, this suffices for a rough approximation of the garment shape but not to predict wrinkles and folds. We therefore use the garment mesh to create *patch-wise features*, that account for the local neighborhood of each garment vertex by using mesh convolution operations [27]. In other words, instead of using a standard PointNet architecture, we use the more sophisticated one depicted by Fig. 3 to compute point-wise, patch-wise, and global features. As can be seen in Fig. 3, the features extracted at each stage are forwarded to the later stages via skip connections. This follows the intuition behind densely connected networks [11] and allows us to directly exploit the low-level information when extracting higher-level representations.

Fusion Network. Once the features are produced by the Garment and Body streams, they are concatenated and given as input to the fusion network (purple box in Fig. 2). It consists of four MLP blocks shared by all the points as in the segmentation network of PointNet [24]. The final MLP block outputs the 3D shifts \mathcal{T}^P in Eq. 1 from the warped garment shape \mathcal{M} .

Variants of our Approach. The Garment stream described above only uses the global body features, because there is no direct correspondence between the body points

and the garment ones. This is where the differences between the two variants of our approach come in.

In the **GarNet-Global** version depicted by Fig. 2(a), we simply discard the point-wise body features and rely exclusively on the global body ones. Note that the local body features are still implicitly used via the global ones that depend on them. By contrast in the **GarNet-Local** version depicted by Fig. 2(b), we explicitly exploit the point-wise body features by introducing a nearest neighbor pooling strategy, shown as a dark blue box, to compute separate local body features for each garment vertex. It takes as input the point-wise body features and uses a nearest neighbor approach to compute additional features that capture the proximity of \mathcal{M} to \mathcal{B} and feeds them into the fusion network, along with the body and garment features.

Fig. 4 depicts the pooling procedure in more detail. It first computes and sorts the Euclidean distance matrix $D \in \mathcal{R}^{M \times N}$ of the M body and N garment locations. D is then used to select the K nearest body vertices for each garment vertex. Finally, the corresponding point-wise body features are max-pooled to obtain the local body features.

3.3. Loss Function

To learn the weights of our network, we minimize the loss function $\mathcal{L}(\mathcal{G}^G, \mathcal{G}^P, \mathcal{B}, \mathcal{M})$. We designed it so as to minimize the distance of the prediction \mathcal{G}^P to the ground truth \mathcal{G}^G while also incorporating regularization terms derived from physical constraints. The latter also depend on the body \mathcal{B} and the garment template \mathcal{M} . We therefore write \mathcal{L} as

$$L_{vertex} + \lambda_{pen} L_{pen} + \lambda_{norm} L_{norm} + \lambda_{bend} L_{bend}, \quad (2)$$

where λ_{pen} , λ_{norm} , and λ_{bend} are weights associated to the individual terms described below. We will study the individual impact of these terms in the results section.

Data Term. We take L_{vertex} to be the average L^2 distance between the vertices of \mathcal{G}^G and \mathcal{G}^P ,

$$\frac{1}{N} \sum_{i=1}^N \|\mathbf{G}_i^G - \mathbf{G}_i^P\|^2, \quad (3)$$

where N is the total number of vertices.

Interpenetration Term. To assess whether a garment vertex is inside the body, we first find the nearest body vertex. At each iteration of the training process, we perform this search for all garment vertices. This yields $\mathcal{C}(\mathcal{B}, \mathcal{G}^P)$, a set of index pairs, one for the garment vertices and the other for the corresponding body vertices. We take the interpenetration term L_{pen} to be

$$\sum_{\{i,j\} \in \mathcal{C}(\mathcal{B}, \mathcal{G}^P)} \mathbb{1}_{\{\|\mathbf{G}_j^P - \mathbf{G}_i^G\| < d_{tol}\}} \text{ReLU}(-\mathbf{N}_{\mathbf{B}_i}^T (\mathbf{G}_j^P - \mathbf{B}_i)) / N, \quad (4)$$

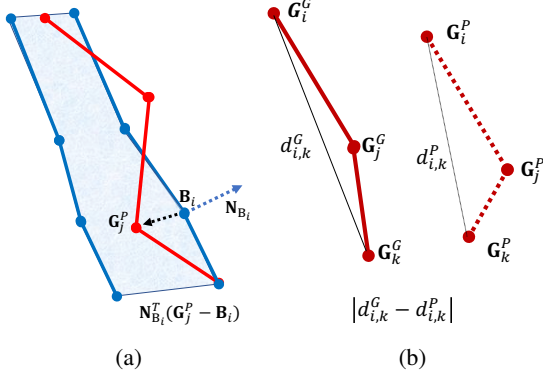


Figure 5: **Interpenetration and Bending loss terms.** (a) The interpenetration term L_{pen} penalizes a garment vertex \mathbf{G}_j^P for being on the wrong side of the corresponding body point \mathbf{B}_i . (b) The bending term L_{bend} penalizes the distance between two neighbors of \mathbf{G}_j^P to differ from that in the ground truth.

to penalize the presence of garment vertices inside the body. Here, \mathbf{N}_{B_i} is the normal vector at the i^{th} body vertex, as depicted by Fig 5(a). This formulation penalizes garment vertices that are on the wrong side of the body mesh, provided that they are less than a distance d_{tol} from their ground-truth position. In other words, the constraint only comes into play when the vertex is sufficiently close to its true position to avoid imposing spurious constraints at the beginning of the optimization. Unlike in DRAPE [9], we do not force the garment vertex to be within a predefined distance of the body because, in some cases, garment vertices can legitimately be far from it.

Normal Term. We write L_{norm} as

$$\frac{1}{N_F} \sum_{i=1}^{N_F} \left(1 - (\mathbf{F}_i^G)^T \mathbf{F}_i^P \right)^2, \quad (5)$$

to penalize the angle difference between the ground-truth and predicted facet normals. Here, N_F , \mathbf{F}_i^G and \mathbf{F}_i^P are the number of facets, the normal vector of the i^{th} ground-truth facet, and the corresponding predicted one, respectively.

Bending Term. We take L_{bend} to be

$$\frac{1}{|\mathcal{N}_2|} \sum_{\{i,k\} \in \mathcal{N}_2} \left| \|\mathbf{G}_i^P - \mathbf{G}_k^P\| - \|\mathbf{G}_i^G - \mathbf{G}_k^G\| \right|, \quad (6)$$

to emulate the bending constraint of NvCloth [20], which is an approximation of the one in [19]. Here, \mathcal{N}_2 denotes a set of pairs of vertices connected by a shortest path of two edges. This term helps preserve the distance between neighboring vertices of a given vertex, as shown in Fig. 5(b). Although it is theoretically possible to consider larger neighborhoods, the number of pairs would grow exponentially.

3.4. Implementation Details

The Garment stream employs 3 mesh convolution operators [27]. They use 1-ring neighborhoods to learn patch-wise features. As the mesh convolution operators rely on trainable parameters to weigh the contribution of neighbors, we always concatenate the input vertex 3D locations to their input vectors so that the network can learn topology dependent convolutions. When using the exact PointNet architecture of [24] in the Body stream, we observed that all point-wise body features converged to the same feature vector, which seems to be due to ReLU saturation. To prevent this, we use leaky ReLUs with a slope of 0.1 and add a skip connection from the output of the first Spatial Transformer Network (STN) to the input of the second MLP block. To use the body features in the Garment stream as shown in Fig. 3, the 512-dimensional global body features are repeated for each garment vertex. For the local body pooling depicted by the dark blue box in Fig. 4, we downscale the 3D body points along with their point-wise features by a factor 10. This is done by average pooling applied to the point-wise body features with a 16 neighborhood size. For the local max-pooling of body features in Fig. 4, the number of neighbors is 15.

To train the network, we use the PyTorch [22] implementation of the Adam optimizer [15] with a learning rate of 0.001. In all the experiments reported in the following section, we empirically set the weights of Eq. 2, λ_{normal} , λ_{pen} and λ_{bend} to 0.3, 1.0 and 0.5, respectively.

4. Experiments

In this section, we evaluate the performance of our framework both qualitatively and quantitatively. We first introduce the evaluation metrics we use, and then conduct extensive experiments, including an ablation study of the loss terms on our dataset to show the validity of our design choices. Finally, we compare our method against the only state-of-the-art method [28] for which the training and testing data is publicly available.

4.1. Evaluation Metrics

We introduce the following two separate quality measures:

$$\mathcal{E}_{dist} = \frac{1}{N} \sum_{i=1}^N \|\mathbf{G}_i^G - \mathbf{G}_i^P\|, \quad (7)$$

$$\mathcal{E}_{norm} = \frac{1}{N_F} \sum_{i=1}^{N_F} \arccos \left(\frac{(\mathbf{F}_i^G)^T \mathbf{F}_i^P}{\|\mathbf{F}_i^G\| \|\mathbf{F}_i^P\|} \right). \quad (8)$$

\mathcal{E}_{dist} is the average vertex-to-vertex distance between the predicted mesh and the ground-truth one, while \mathcal{E}_{norm} is the average angular deviation of the predicted facet normals

to the ground-truth ones. Note that, as discussed in [4], the normals are important because they are key to the appearance of the rendered garment.

4.2. Analysis on our Dataset

We created a large dataset featuring many different poses and body shapes. We first explain how we built it and then test various aspects of our framework on it.

Dataset Creation. We used the Nvidia physics-based simulator NvCloth [20] to fit four different garments—female jeans, male jeans, female T-shirt, and male T-shirt represented by 3D triangulated meshes with 5351, 5351, 5278, and 5442 vertices, respectively—on bodies from the CAESAR dataset [1], each of which is represented as a 6449-vertex mesh.

Each body in the CAESAR dataset comes in only one pose, generally the T-pose. To incorporate a variety of poses in our dataset, we animated these bodies with CMU mocap [5] yoga, dance, monkey, and walking motions. We selected 25 poses for each activity and ran the simulator for all 4 garments on each. Due to simulation failures, however, we had to exclude the yoga motion for the jeans.

Since the garment has a fixed size, we first had to prune the CAESAR dataset to only keep the bodies that the garment can fit to realistically. To this end, we uniformly sampled the CEASAR bodies in the interval of 0.8 and 1.4 m of belt circumference, leaving us with 80 female and 98 male bodies in total. Finally, for each *gender-garment* combination, we selected 60% of the body shapes for training, 20% for validation, and 20% for testing.

Quantitative Results. Recall from Section 3.2 that we implemented two variants of our network, **GarNet-Global** that relies solely on global body-features and **GarNet-Local** that also exploits local body-features by performing nearest neighbor pooling as shown in Fig. 2. For completeness, we also implemented a third variant that is a simplified version of **GarNet-Global** in which we removed the mesh convolution layers that produce patch-wise garment features. It therefore performs only point-wise operations, and we dub it **GarNet-Naive**, which can also be interpreted as a two-stream PointNet with extra skip connections. We trained a separate network for each one of the three variants and for each *gender-garment* pair on all training poses.

	T-shirt (F)	Jeans (F)	T-shirt (M)	Jeans (M)
	$\mathcal{E}_{dist}/\mathcal{E}_{norm}$	$\mathcal{E}_{dist}/\mathcal{E}_{norm}$	$\mathcal{E}_{dist}/\mathcal{E}_{norm}$	$\mathcal{E}_{dist}/\mathcal{E}_{norm}$
GarNet-Local	1.45/11.05	1.37/ 8.46	1.62/12.63	1.24/11.54
GarNet-Global	1.57/11.27	1.34/8.52	1.57/12.61	1.29/11.84
GarNet-Naive	2.18/13.95	2.54/14.86	4.04/23.86	1.40/12.62
DQS [13]	5.20/25.23	6.30/22.22	5.52/24.53	4.47/19.40

Table 1: Average distance in cm and face normal angle difference in degrees between the GT and predicted vertices.



Figure 6: **Comparison on the female T-shirt.** The top and bottom rows are from walking and monkey motions, respectively. **GarNet-Naive** produces artifacts near the shoulder while **GarNet-Local** and **PBS** yield similar results. The **GarNet-Global** results are not shown because they are visually indistinguishable from the **GarNet-Local** ones.

	GarNet-Local	GarNet-Global	GarNet-Naive	PBS
time (ms)	44.9	34.7	0.9	2064.8

Table 2: Comparison of the computation time on the female T-shirt dataset. We use a single Nvidia TITAN X GPU for our PBS and the forward propagation of the network with a batch size of 8.

In Table 1, we report our results in terms of the \mathcal{E}_{dist} and \mathcal{E}_{norm} of Section 4.1. In Fig. 7, we plot the corresponding average precision curves for T-shirts and jeans. The average precision is the percentage of vertices/normals of all test samples whose error is below a given threshold. **GarNet-Naive** does worse than the two others, which underlines the importance of patch-wise garment features. **GarNet-Local** and **GarNet-Global** yield comparable results with a slight overall advantage to **GarNet-Local**. Interestingly, the former does noticeably better on the male jeans and the female T-shirt, about the same on the female jeans, and slightly worse on the male T-shirt. Note that the male T-shirt wrinkles less to the flatter shape of the upper body. Similarly, women jeans are tighter on the body by design, also resulting in fewer wrinkles. We interpret this to mean that, without wrinkles, nearest neighbor pooling is not as useful as when wrinkles appear. Finally, in Table 2, we report the computation times of our network models and the employed PBS software. Note that both variants of our approach yield a speedup of more than 40 times.

Qualitative Results. Fig. 6 contrasts the results of the **GarNet-Local** and **GarNet-Naive** architectures. The **GarNet-Global** results are visually indistinguishable from the **GarNet-Local** ones on the printed page. Note that **GarNet-Naive** generates some clearly visible artifacts, such as spurious wrinkles near the right shoulder. By contrast, **GarNet-Local** delivers results that closely match those of the PBS method while being much faster. We provide further evidence of this in Fig. 9.

Ablation study. We conducted a set of experiments on the female T-shirt dataset to highlight the influence of the dif-

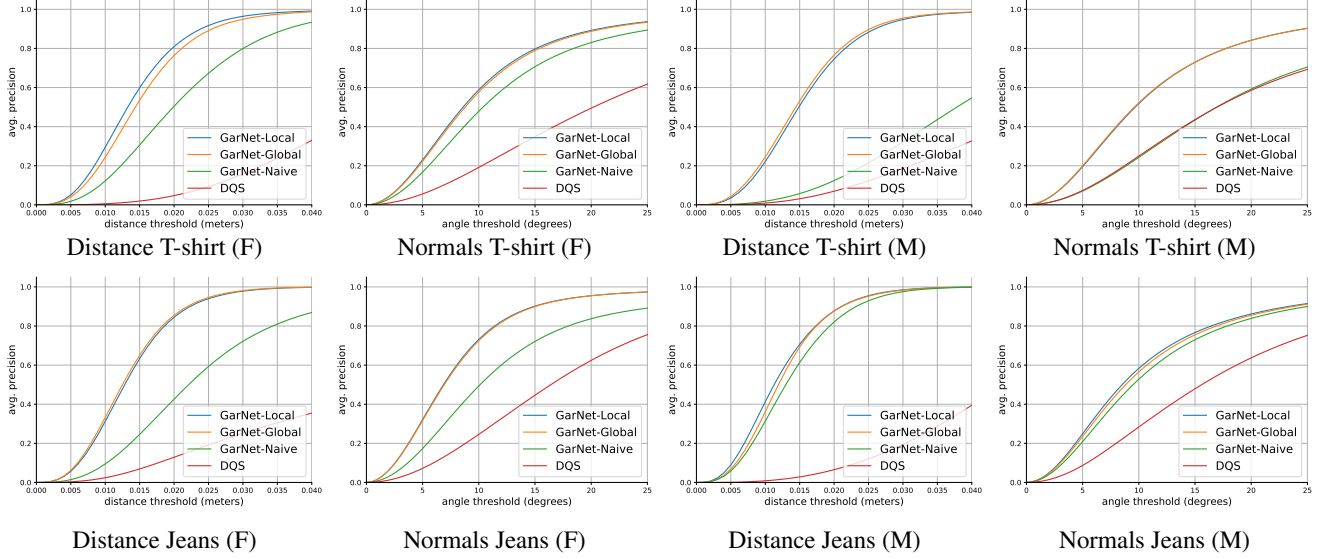


Figure 7: Average precision curves for the vertex distance and the facet normal angle error.

Loss Function	\mathcal{E}_{dist}	\mathcal{E}_{normal}
$L_{vertex} + L_{pen}$	1.29	16.52
$L_{vertex} + L_{pen} + L_{bend}$	1.36	15.43
$L_{vertex} + L_{pen} + L_{norm} + L_{bend}$	1.45	11.05
$L_{vertex} + L_{norm} + L_{bend}$	1.47	11.24
$L_{vertex} + L_{pen} + L_{norm}$	1.92	11.42

Table 3: Ablation study on the female T-shirt dataset.

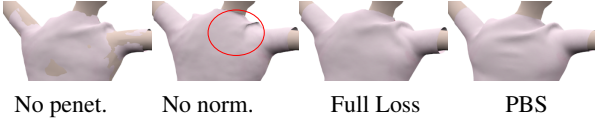


Figure 8: **Ablation study.** Reconstruction without some of the loss terms results in interpenetration (left) or artifacts near the shoulder (second from left). By contrast using the full loss yields a result very similar to the PBS one (two images on the right).

ferent terms in our loss function. To this end, we trained the network by individually removing the penetration term, the bending term, and the normal term. We also report results without both the normal and bending terms. As shown in Table 3, using the normal and bending terms significantly improves the fitting accuracy. This is depicted in Fig. 8 where the red circle indicates how the normal term improves wrinkle prediction. While removing the penetration term only has limited impact on the quantitative results, it causes much more severe interpenetration, as also shown in Fig. 8. To gauge the effectiveness of the interpenetration term L_{pen} of Eq. 4, we also measure the average percentage of garment vertices that fall within the body mesh by using the sign of $\mathbf{N}_{B_i}^T (\mathbf{G}_j^P - \mathbf{B}_i)$. This percentage falls from 20.1% to 6.5%

	GarNet-Local	GarNet-Global	GarNet-Naive	[28]
Dist. %	0.87	0.95	5.02	3.01

Table 4: Distance % error on the shirt dataset of [28].

in the test set when turning on L_{pen} .

4.3. Comparative Results on the Dataset of [28]

As discussed in Section 2, [28] is the only non-PBS method that addresses a problem similar to ours and for which the data is publicly available. Specifically, the main focus of [28] is to drape a garment on several body shapes for different garment sewing patterns. Their dataset contains 7000 samples consisting of a body shape in the T-pose, garment parameters, and the fitted garment. Hence, the inputs to the network are the body shape, or its parameters, and the garment sewing parameters. To use **GarNet** for this purpose, we concatenated the garment sewing parameters to each vertex before feeding them to the MLP blocks of our network. We take one of the fitted garments from the training set to be the template input to our network.

We use the same training (95%) and test (5%) splits as in [28] and compare our results with theirs in terms of the normalized L^2 distance percentage, that is, $100 \times \frac{\|G^G - G^P\|}{\|G^G\|}$ where G^G and G^P are the vectorized ground-truth and predicted vertex locations normalized to the range [0, 1]. We use this metric here because it is the one reported in [28]. As evidenced by Table 4, our architectures perform significantly better.

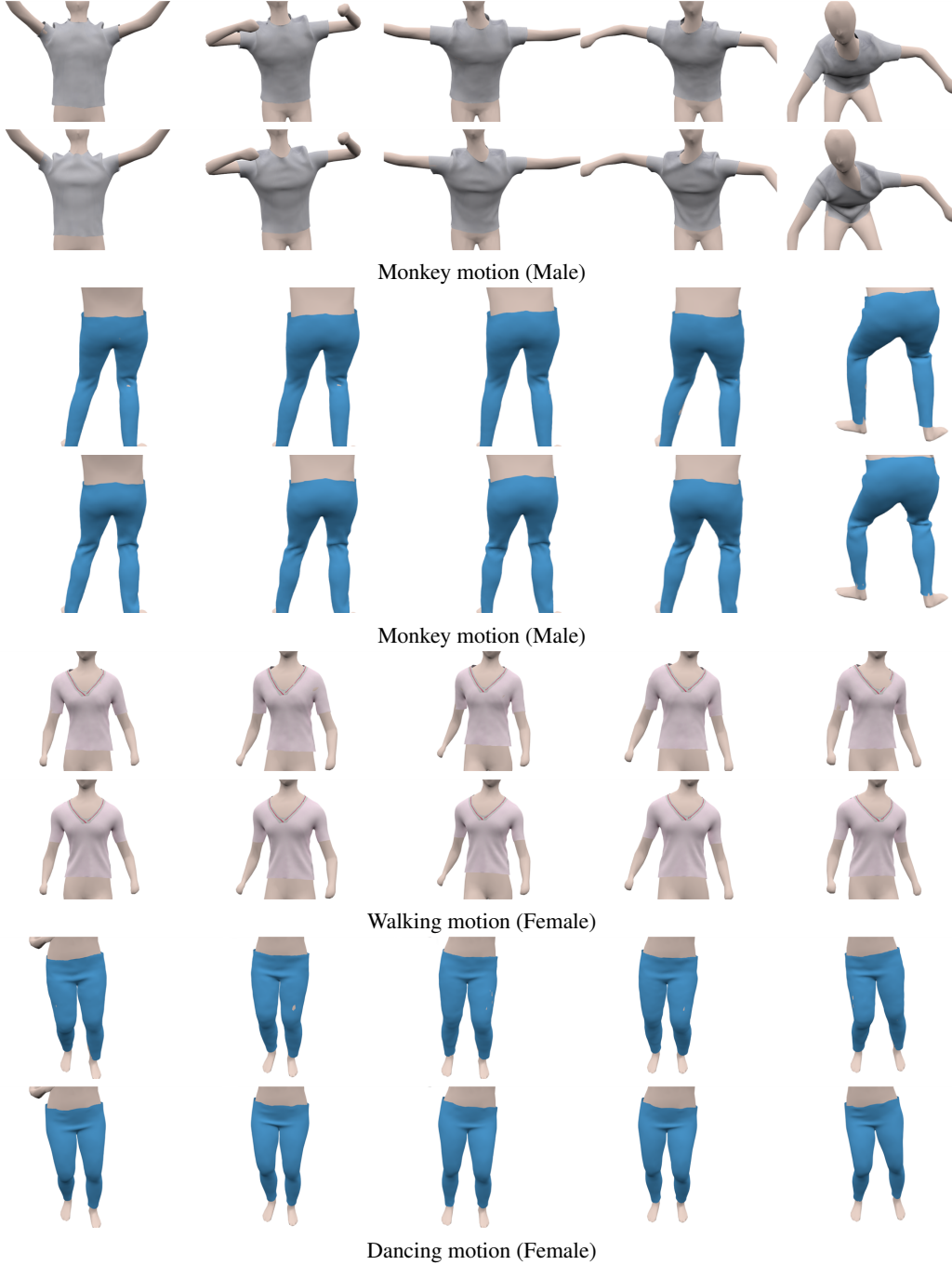


Figure 9: **GarNet vs PBS results for several body poses and garment-gender combinations.** In all row pairs, we compare the **GarNet** results (top) and the **PBS** ones (bottom). Note how similar they are, even though the former were computed in approx. 50ms instead of 2s.

5. Conclusion

In this work, we have introduced a new two-stream network architecture that can drape a 3D garment shape on different target bodies in many different poses, while running 40 times faster than a physics-based simulator. Its key elements are an approach to jointly exploiting body and gar-

ment features early in the process and a loss function that promotes the satisfaction of physical constraints.

Although our model can predict the fitted garment shapes to within 1.5 cm average distance from the ground truth while limiting interpenetrations and other artifacts, it still has a tendency to remove high frequency details. A promising approach to addressing this problem was introduced

in [2] for face reconstruction purposes: This algorithm did not attempt to precisely capture the very fine structure of the skin; instead it added noise with similar statistics that is virtually indistinguishable from the ground truth to the human eye. In future work, we will explore the use of conditional Generative Adversarial Networks [12] to add subtle wrinkles that will further increase the realism of our reconstructions as in [16].

References

- [1] B. Allen, B. Curless, and Z. Popović. The Space of Human Body Shapes: Reconstruction and Parameterization from Range Scans. In *ACM SIGGRAPH 2003 Papers*, pages 587–594, 2003. 2, 6
- [2] T. Beeler, B. Bickel, P. Beardsley, B. Sumner, and M. Gross. High-Quality Single-Shot Capture of Facial Geometry. *ACM SIGGRAPH*, 29(3), 2010. 9
- [3] D. Boscaini, J. Masci, E. Rodolà, and M. Bronstein. Learning Shape Correspondence with Anisotropic Convolutional Neural Networks. In *Advances in Neural Information Processing Systems*, pages 3189–3197, 2016. 3
- [4] R. Brouet, A. Sheffer, L. Boissieux, and M.-P. Cani. Design Preserving Garment Transfer. *ACM Trans. Graph.*, 31(4):361–3611, July 2012. 2, 6
- [5] CMU Graphics Lab Motion Capture Database, 2010. <http://mocap.cs.cmu.edu/>. 6
- [6] H. Deng, T. Birdal, and S. Ilic. PPFNet: Global Context Aware Local Features for Robust 3D Point Matching. In *Conference on Computer Vision and Pattern Recognition*, 2018. 3
- [7] M. Designer, 2018. <https://www.marvelousdesigner.com>. 2
- [8] P. Guan, O. Freifeld, and M. J. Black. A 2D Human Body Model Dressed in Eigen Clothing. In *European Conference on Computer Vision*, pages 285–298, 2010. 2
- [9] P. Guan, L. Reiss, D. Hirshberg, A. Weiss, and M. J. Black. DRAPE: Dressing Any Person. *ACM Trans. on Graphics (Proc. SIGGRAPH)*, 31(4):351–3510, July 2012. 2, 5
- [10] H. W. F. Hecht, R. Ramamoorthi, and J. O’Brien. Example-Based Wrinkle Synthesis for Clothing Animation. In *ACM SIGGRAPH*, 2010. 2
- [11] G. Huang, Z. Liu, K. Weinberger, and L. van der Maaten. Densely Connected Convolutional Networks. In *Conference on Computer Vision and Pattern Recognition*, 2017. 4
- [12] S. Isola, J. Zhu, T. Zhou, and A. Efros. Image-To-Image Translation with Conditional Adversarial Networks. In *Conference on Computer Vision and Pattern Recognition*, 2017. 9
- [13] L. Kavan, S. Collins, J. Žára, and C. O’Sullivan. Skinning with Dual Quaternions. In *Proceedings of the 2007 Symposium on Interactive 3D Graphics and Games*, pages 39–46, 2007. 3, 6
- [14] T.-Y. Kim and E. Vendrovsky. Drivenshape - A Data-Driven Approach for Shape Deformation. In *Eurographics/SIGGRAPH Symposium on Computer Animation*, 2008. 2
- [15] D. P. Kingma and J. Ba. Adam: A Method for Stochastic Optimization. *arXiv Preprint*, 2014. 5
- [16] Z. Lahner, D. Cremers, and T. Tung. Deepwrinkles: Accurate and Realistic Clothing Modeling. In *European Conference on Computer Vision*, September 2018. 2, 9
- [17] J. Masci, D. Boscaini, M. M. Bronstein, and P. Vandergheynst. Geodesic Convolutional Neural Networks on Riemannian Manifolds. In *International Conference on Computer Vision*, pages 832–840, December 2015. 3
- [18] F. Monti, D. Boscaini, J. Masci, E. Rodolà, J. Svoboda, and M. M. Bronstein. Geometric Deep Learning on Graphs and Manifolds Using Mixture Model CNNs. In *Conference on Computer Vision and Pattern Recognition*, pages 5425–5434, 2017. 3
- [19] M. Miller, B. Heidelberger, M. Hennix, and J. Ratcliff. Position Based Dynamics. *Journal of Visual Communication and Image Representation*, 18(2):109–118, 2007. 5
- [20] Nvidia. Nvcloth, 2018. <https://docs.nvidia.com/gameworks/content/gameworkslibrary/physx/nvCloth/index.html>. 2, 5, 6
- [21] Nvidia. Nvidia flex, 2018. <https://developer.nvidia.com/flex>. 2
- [22] A. Paszke, S. Gross, S. Chintala, G. Chanan, E. Yang, Z. DeVito, Z. Lin, A. Desmaison, L. Antiga, and A. Lerer. Automatic Differentiation in Pytorch. In *Advances in Neural Information Processing Systems*, 2017. 5
- [23] G. Pons-Moll, S. Pujades, S. Hu, and M. J. Black. Clothcap: Seamless 4D Clothing Capture and Retargeting. *ACM Trans. Graph.*, 36(4):731–7315, July 2017. 2
- [24] C. Qi, H. Su, K. Mo, and L. Guibas. Pointnet: Deep Learning on Point Sets for 3D Classification and Segmentation. In *Conference on Computer Vision and Pattern Recognition*, 2017. 1, 3, 4, 5
- [25] C. Qi, L. Yi, H. Su, and L. Guibas. Pointnet++: Deep Hierarchical Feature Learning on Point Sets in a Metric Space. In *Advances in Neural Information Processing Systems*, 2017. 3
- [26] O. F. D. Software, 2018. <https://optitex.com/>. 2
- [27] N. Verma, E. Boyer, and J. Verbeek. Feastnet: Feature-Steered Graph Convolutions for 3D Shape Analysis. In *Conference on Computer Vision and Pattern Recognition*, 2018. 3, 4, 5
- [28] T. Y. Wang, D. Ceylan, J. Popovic, and N. J. Mitra. Learning a shared shape space for multimodal garment design. In *ACM SIGGRAPH Asia*, 2018. 2, 5, 7
- [29] Y. Yang, C. Feng, Y. Shen, and D. Tian. Foldingnet: Point Cloud Auto-Encoder via Deep Grid Deformation. In *Conference on Computer Vision and Pattern Recognition*, June 2018. 3
- [30] K. M. Yi, E. Trulls, Y. Ono, V. Lepetit, M. Salzmann, and P. Fua. Learning to Find Good Correspondences. In *Conference on Computer Vision and Pattern Recognition*, 2018. 3
- [31] L. Yu, X. Li, C. Fu, D. Cohen-Or, and P. Heng. Pu-Net: Point Cloud Upsampling Network. In *Conference on Computer Vision and Pattern Recognition*, pages 2790–2799, 2018. 3